

## Duplications of a model prebiotic iron-sulphur tripeptide leads to the formation of a protoferredoxin

Simone Scintilla<sup>a</sup>, Claudia Bonfio<sup>a</sup>, Luca Belmonte<sup>a</sup>, Michele Forlin<sup>a</sup>, Daniele Rossetto<sup>a</sup>, Jingwei Li<sup>b</sup>, James A. Cowan<sup>b</sup>, Angela Galliani<sup>c</sup>, Fabio Arnesano<sup>c</sup>, Michael Assfalg<sup>d</sup>, Sheref S. Mansy<sup>\*a</sup>

<sup>a</sup>CIBIO, University of Trento, Via Sommarive 9, 38123 Povo, Italy

<sup>b</sup>Department of Chemistry and Biochemistry, the Ohio State University, 100 West 18th Ave, Columbus, OH 43210, USA

<sup>c</sup>Department of Chemistry, University of Bari "A. Moro", via E. Orabona 4, 70125 Bari, Italy.

<sup>d</sup>Department of Biotechnology, University of Verona, Strada Le Grazie 15, 37134 Verona, Italy.

The Supplementary Information contains:

Supplementary Methods

Supplementary Tables 1-3

Supplementary Figures S1-S19

## Supplementary Methods

**Materials.** All reagents were from Sigma Aldrich and used without any further purification. MilliQ water was distilled under nitrogen flow to deoxygenate the solvent. The synthetic procedures to obtain the cluster were performed under controlled nitrogen atmosphere with a Schlenk line and Schlenk glassware. The products were maintained under nitrogen (or argon) inert atmosphere and transferred to NMR tubes capped with rubber septa, anaerobic sealed Hellma quartz cuvettes, or sealed glass vials for NMR, UV-Visible spectroscopy, and mass spectrometry, respectively.

**EPR spectroscopy.** Low temperature EPR spectra were collected at the Ohio Advanced EPR Laboratory at Miami University on a Bruker EMX spectrometer equipped with an Oxford cryostat and ER 4116DM dual mode resonator. Experimental parameters were as follows: temperature, 20, 40, 80 K; microwave frequency, 9.619 GHz; microwave power, 10 mW; modulation amplitude, 10 G; modulation frequency, 100 kHz, time constant, 40.96 ms; conversion time, 40.96 ms; number of scans, 20, number of points, 1024.

**NMR spectroscopy.** NMR spectra were recorded at 25 °C using a 600 MHz Bruker Avance III spectrometer equipped with a triple resonance TCI cryogenic probe. Typical one-dimensional  $^1\text{H}$ -NMR spectra were acquired with an excitation sculpting water suppression pulse sequence that utilizes water selective  $180^\circ$  pulses. Acquisition parameters were 16 scans, 29761 Hz (50 ppm) spectral width, 4 s recycle delay, 0.550 s acquisition time, 32768 time domain data points. Exponential filtering of 1 Hz was applied prior to Fourier transformation. After Fourier transformation, the spectra were phase- and baseline-corrected manually. One-dimensional  $^1\text{H}$ -NMR spectra optimized for paramagnetic samples were acquired with a water presaturation pulse sequence. A low power (50 Hz RF field) pulse was applied during the 0.08 s recycle delay. Acquisition parameters were 24 scans, 178571 Hz (298 ppm), 0.004816 s acquisition time, 1720 data points. The free induction decay was processed using 400 Hz exponential filtering prior to Fourier transformation (2048 points). For resonance assignment, two-dimensional  $^1\text{H}$  homonuclear chemical shift correlation spectroscopy (COSY) and  $^1\text{H}$ - $^{13}\text{C}$  heteronuclear single quantum correlation (HSQC) experiments

were used. Magnitude-mode multiple quantum filtered COSY spectra were acquired with presaturation of the water resonance during the recycle delay (2 s) using the following parameters: 16 scans, 2048 (F2, direct dimension) and 240 (F1, indirect dimension) data points, 7812 Hz (13 ppm) spectral width in both F1 and F2, 0.131 s acquisition time. The spectra were processed applying a  $\pi/3$ -shifted squared sine-bell function in both dimensions and zero-filling to a final spectrum size of 2048  $\times$  1024 data points. HSQC experiments were acquired with a phase-sensitive standard pulse sequence incorporating a sensitivity-improvement scheme, shaped pulses for inversion, and gradients in the back-INEPT sequence.  $^{13}\text{C}$  decoupling from  $^1\text{H}$  was obtained by applying a GARP4 pulse train (decoupling pulse length 60  $\mu\text{s}$ ) during acquisition. Additional acquisition parameters were 16 scans, 1024 (F2, direct dimension) and 192 (F1, indirect dimension) data points, 9615 Hz (16 ppm, F2) and 30180 Hz (200 ppm, F1, centered at 70 ppm) spectral widths, 2 s recycle delay, 145 Hz  $^1\text{H}$ - $^{13}\text{C}$  coupling constant, and 500  $\mu\text{s}$  pulse length of adiabatic inversion pulse. The spectra were processed applying a  $\pi/2$ -shifted sine-bell function in both dimensions and zero-filling to a final spectrum size of 1024  $\times$  512 data points.

**Mass spectrometry.** ESI-MS analyses of freshly prepared aqueous solutions of free peptide and peptide complexed with iron and sulfide were performed with a dual electrospray interface and a quadrupole time-of-flight mass spectrometer (Agilent 6530 Series Accurate-Mass Quadrupole Time-of-Flight (Q-TOF) LC/MS). The samples were injected at a rate of 10  $\mu\text{L}/\text{min}$ . Ionization was achieved in the positive ion mode by application of +3.5 kV at the entrance of the capillary. The pressure of the nebulizer gas was 35 psig. The drying gas was heated to 300  $^\circ\text{C}$  at a flow rate of 8 L/min. Full mass spectra were recorded in the mass/charge (m/z) range of 100-2000.

**UV-Visible spectroscopy.** UV-Visible absorption spectra of freshly prepared solutions were recorded with an Agilent 8453 UV-Visible diode array spectrophotometer with an integration time of 0.5 s and an interval of 1 nm.

**Spectral decomposition and [2Fe-2S] half life estimation.** Any given UV-Visible spectrum ( $y$ ) was fit to the mixed sum of four reference spectra ( $s_1, s_2, s_3, s_4$ ) using the least squares method:

$$y = p_1 \cdot s_1 + p_2 \cdot s_2 + p_3 \cdot s_3 + p_4 \cdot s_4$$

Parameters were constrained to be null or positive. After parameter normalization, such that

$$p_1 + p_2 + p_3 + p_4 = 1, \text{ each one of the four estimated parameters represented an approximation of the}$$

contribution of the corresponding species to the overall UV-Visible spectrum. The four UV spectra

corresponding to the species [2Fe-2S] -both oxidized and reduced-, S-coordinated glutathione/Fe

mononuclear complex and O-coordinated glutathione/Fe complex used for the spectral decomposition are reported in Fig. S1.

The half-life of the [2Fe-2S] cluster was estimated by fitting the [2Fe-2S] cluster overall contribution (addition of both reduced and oxidized parameters) over time. After an initial peak, a decreasing regime brought the curve to a plateau. The decreasing regime was fit to one of the following equations, depending on the features of its curve profile:

$$(1) [2Fe - 2S](t) = \frac{A_1 - A_2}{1 + e^{(t-t_0)/dt}} + A_2$$

$$(2) [2Fe - 2S](t) = [2Fe - 2S](0) + Ae^{-t/\tau}$$

The half-life  $t_{1/2}$  could then be estimated as:

$$(1) t_{1/2} = t_0$$

$$(2) t_{1/2} = \tau \ln(2)$$

All data analyses and estimations were calculating using R statistical computing software.<sup>1</sup>

**Peptide stabilized iron-sulfur cluster synthesis.** Unless otherwise noted, sodium sulfide ( $\text{Na}_2\text{S}\cdot 9\text{H}_2\text{O}$ , 1.29  $\mu\text{mol}$ , 0.185 mM) was added to an aqueous solution containing peptide (280  $\mu\text{mol}$ , 40 mM) at pH 8.6 in a Schlenk round bottom flask under anaerobic conditions. Subsequently, ferric chloride ( $\text{FeCl}_3\cdot 6\text{H}_2\text{O}$ , 3.5  $\mu\text{mol}$ , 500  $\mu\text{M}$ ) was added to obtain [2Fe-2S] peptide. The pH screening used 0.185 mM sodium sulfide, 0.5 mM ferric chloride, and 40 mM glutathione under the same synthetic procedure but under different solution pH (between pH 6 and 11). Glutathione concentration screening used 0.185 mM sodium sulfide, 0.5 mM ferric chloride, and 10-80 mM glutathione. Sulfide screening used 40 mM glutathione, 0.5 mM ferric chloride, and 0.05-0.5 mM sodium sulfide. Iron screening used 40 mM glutathione, 0.185 mM sodium sulfide, and 0.05-2.0 mM ferric chloride. The influence of NaCl and  $\text{MgCl}_2$  on cluster formation and stability was assessed by adding 0-500 mM NaCl or  $\text{MgCl}_2$  to 40 mM glutathione prior to the addition of 0.185 mM sodium sulfide and 0.5 mM ferric chloride. Mononuclear complexes were obtained by adding  $\text{FeCl}_3$  (0.5 mM, 3.5  $\mu\text{mol}$ ) to glutathione (40 mM, 280  $\mu\text{mol}$ , pH 8.6). Oxidized glutathione coordinated to iron was obtained by halving the glutathione concentration, i.e. 20 mM glutathione and 0.5 mM ferric chloride. The spectrum of reduced [2Fe-2S] glutathione was collected after [2Fe-2S] glutathione was incubated at room temperature for over 180 min or by addition of 0.5 mM ferric chloride to a mixture 40 mM glutathione and 0.5mM sodium sulfide, pH 8.6.

**FPLC chromatography.** [2Fe-2S] glutathione was loaded with a 500  $\mu\text{L}$  loop onto glutathione conjugated agarose resin (GSTrap HP, 1 mL bed volume, GE Healthcare) connected to an ÄKTA purifier P-900 system with a Frac-920 fraction collector. The flow rate was 0.5 mL/min. The running buffer was either 40 mM glutathione, pH 8.6 or water brought to pH 8.6. Eluate was monitored at 405 nm.

**UV-Visible monitored reduction and oxidation.** 1 mL of a solution containing [2Fe-2S] glutathione (40 mM glutathione, 0.185 mM sodium sulfide, 0.5 mM ferric chloride, pH 8.6; estimated cluster concentration 93  $\mu\text{M}$ ) was transferred to an anaerobic cuvette under inert  $\text{N}_2$  atmosphere and a UV-Visible absorption spectrum was collected. For the reduction step, 2  $\mu\text{L}$  of an aqueous solution containing the reducing agent

sodium dithionite was added (0.05  $\mu\text{mol}$ , 50  $\mu\text{M}$ ) and the UV-Visible absorption spectrum was collected immediately after mixing. Next, 2  $\mu\text{L}$  of an aqueous solution containing the oxidizing agent hydrogen peroxide (0.05  $\mu\text{mol}$ , 50  $\mu\text{M}$ ) was added and the UV-Visible absorption spectrum was immediately collected after mixing. For repeated cycles of reduction-oxidation, the same amount of reductant or oxidant as indicated above was repeatedly added until the reduced or oxidized state of [2Fe-2S] glutathione was observed by UV-Visible absorption spectrum.

Freshly prepared, sodium dithionite reduced [2Fe-2S] glutathione was also purified under inert  $\text{N}_2$  atmosphere with a Sephadex G-10 column with 40mM glutathione solution, pH 8.6 running buffer. The eluate was then transferred to a vacuum cuvette, and the UV-visible absorption spectrum was collected. Subsequently, the solution in the cuvette was oxidized by the addition of hydrogen peroxide, and the UV-Visible absorption spectrum collected.

**Iron-sulfur cluster stability.** [2Fe-2S] clusters were synthesized with a fixed amount of sodium sulfide (0.1 mM) and ferric chloride (0.25 mM) in the presence of different concentrations of ligand, i.e. glutathione, hexapeptide, or dodecapeptide. The concentrations of cysteinyl ligand were 20 mM, 10 mM, 5 mM, 2.5 mM, and 1 mM. Complexes were monitored over time by UV-Visible spectrophotometry and decomposed as described above.

**Solid phase peptide synthesis.** The synthesis of glutathione polymers was as previously described.<sup>2,3</sup> *N,N*-dimethyl formamide (DMF) was used as the solvent and preloaded fluorenylmethyloxycarbonyl-glycyl Wang resin (Fmoc-Gly Wang) was used as the starting polymeric support. Trityl-protected Fmoc-Cysteine (Fmoc-Cys(Trt)OH), tert-butyl-protected Fmoc-Glutamic acid (Fmoc-Glu-OtBu), and Fmoc-Glycine (Fmoc-Gly-OH) were used as building blocks. In general, the peptide chain was elongated by sequential Fmoc deprotection of the residue anchored to the resin and Fmoc-AA-OH (AA = Cys, Glu and Gly, in sequence) coupling. Fmoc deprotection was obtained by washing the mixture with 20% (v/v) solution of piperidine in DMF. For each coupling, an excess (Fmoc-AA-OH: anchored AA, 3:1) of the Fmoc- $\alpha$ -amino acid derivative was added to the resin. Apart from Fmoc-Cys(Trt)-OH, Fmoc- $\alpha$ -amino acid derivatives were activated with a

mixture of hydroxyl-benzotriazole (HOBt), *N,N,N',N'*-tetramethyl-O-(benzotriazol-1-yl)uronium tetrafluoroborate (TBTU), and *N,N*-diisopropylethyl amine (DIPEA). Fmoc-Cys(Trt)OH was activated with a *N,N'*-diisopropylcarbodiimide (DIC)/HOBt mixture. At the end of the coupling, the polymers were cleaved from the resin and deprotected by treatment with a solution of trifluoroacetic acid (TFA):H<sub>2</sub>O:triisopropyl silane (TIS):1,2-ethanedithiol (EDT) (volume ratio 37:1:1:1) for 2 h. The volume was successively reduced under nitrogen atmosphere to avoid cysteinyl-thiol oxidation, and the product was precipitated with a cold solution of diethyl ether/petroleum ether (30:70% (v/v)) followed by washing cycles with diethyl ether or extracted 3 times with 20% acetic acid/chloroform and finally dried under inert atmosphere.

**Density Functional Theory Calculations.** An approach similar to that of Kaszuba et al. was exploited.<sup>4</sup> Cluster coordinates up to the  $\beta$ -carbons of cysteines were taken from the PDB ID 2WUL. Calculations were run with GAMESS-US<sup>5</sup> and evaluated with MacMolPlot<sup>6</sup> while the missing aliphatic hydrogens were introduced with Avogadro.<sup>7</sup> Initial geometry optimization was by the linear combination of the atomic orbitals (LCAO) of the irons, sulfides, and ligands with the Combo package of PC-Gamess Firefly.<sup>8</sup> Since the triple- $\xi$  basis set plus polarization was needed to accommodate the transition metals<sup>9,10</sup>, geometry optimization was carried out at the B3LYP/6-3 11G(2d,p) level of theory for the ligands. All electrons Ahlrichs VTZ<sup>11</sup> basis set was used for the metals (downloaded from Basis Set Exchange EMSL<sup>12,13</sup>). The high spin state was obtained with the Unrestricted Hartree Fock method. A second step of geometry optimization using solvent water used the Polarizable Continuum Model (PCM).<sup>14</sup> Metal Ionic radii were from a previous report.<sup>15</sup> The antiferro-magnetic coupling was taken into account by the broken symmetry approach.<sup>16</sup> The optimized geometry was used for both the Hessian matrix calculation and for the charge fitting. The parameters for bonds, angle, and dihedral force constants were calculated using a previously described method.<sup>17</sup> The Merz-Kollman method<sup>18,19</sup> for Molecular Electrostatic Potential was used. Calculated charges of both [2Fe-2S] cluster and methanethiolates groups were remapped into our customized version of the Charmm Force Field<sup>20,21,22</sup> along with the force constants obtained from the previous geometry optimization. Avogadro was used to manipulate GAMESS-US input files.

**Molecular Dynamics.** Molecular Dynamics was performed with NAMD<sup>23</sup> using our customized version of the Charmm Force Field. Coordinates for two glutathiones and one [2Fe-2S] were from a previously deposited structure (PDB ID: 2WUL) and manipulated with UCSF Chimera<sup>24</sup> to build a [2Fe-2S] coordinated by four molecules of glutathione. The system was solvated in standard TIP3 water and then neutralized with NaCl using Periodic Boundary Conditions. The complete system was equilibrated for 150 ps and subsequently heated to 298 K at a constant pressure of 1 atm. The calculation interval for the equations of motion was 1 fs. The SHAKE<sup>25</sup> algorithm was used to constrain all bonds of hydrogen atoms. Non-bonded energy terms were calculated from 10 to 12 Å with smoothing cut-off functions for both the electrostatics and van der Waals forces. The Ewald sum was computed using the Particle-Mesh Ewald (PME)<sup>26</sup> while the Langevin algorithm was used for temperature and pressure control of the NPT ensemble. Simulations ran for 10 ns. Analyses of the trajectories were performed using VMD.<sup>27</sup> Complexes were considered stable on the base of the RMSD of the trajectory and related histograms.<sup>28</sup> Hydrogen bonds were identified with HBPLUS<sup>29</sup> by using a maximum distance of 3.1 Å and a default maximum donor-hydrogen-acceptor angle of 90°. For local contacts the default distance of 3.9 Å was used.

Trajectory Coverage	Frequency	1st Residue Number	1st Residue Name	1st Interacting Atom	2nd Residue Number	2nd Residue Name	2nd Interacting Atom
100%	6001	11	CYS	N	10	GLU	O
	6001	8	CYS	N	7	GLU	O
	6001	5	CYS	N	4	GLU	O
	6001	2	CYS	N	1	GLU	O
>50%	3405	7	GLU	N	4	GLU	O
>30%	2619	10	GLU	OT1	1	GLU	N
	2462	10	GLU	OT2	1	GLU	N
>10%	1798	3	GLY	N	1	GLU	O
	1692	7	GLU	N	3	GLY	OT1
	1444	7	GLU	OT2	4	GLU	O
	1390	7	GLU	N	3	GLY	OT2
	1038	10	GLU	N	9	GLY	OT1
	979	12	GLY	N	10	GLU	O
	954	10	GLU	N	9	GLY	OT2
	663	7	GLU	OT2	4	GLU	N
<10%	382	7	GLU	N	4	GLU	OT2
	381	11	CYS	O	9	GLY	OT1
	318	3	GLY	OT1	1	GLU	O
	315	11	CYS	O	9	GLY	OT2
	269	12	GLY	OT2	11	CYS	O
	260	3	GLY	OT2	1	GLU	O
	239	6	GLY	OT2	5	CYS	O
	222	10	GLU	OT2	1	GLU	OT1

	216	4	GLU	OT2	3	GLY	OT1
	211	2	CYS	O	1	GLU	N

**Supplementary Table 1. List of electrostatic contacts recorded by means of HBPlus over the MD**

**trajectory.** On the basis of the RMSD, the first 4 ns of the trajectory was removed, resulting in 6001 frames.

Only a small portion of the atoms interact for the entire trajectory. Interactions with low frequencies (<200 hits ~ 3%) are omitted for the sake of clarity. OTX indicates carboxylate oxygens.

Frequency	Donor Number	Donor Name	Donor Atom	Acceptor Number	Acceptor Name	Acceptor Atom
149	1	GLU	N	2	CYS	O
6	12	GLY	N	10	GLU	O
4	8	CYS	N	2	CYS	SG

**Supplementary Table 2. List of hydrogen bonds recorded by means of HBPlus.** As opposed to the

electrostatic contacts listed in Supplementary Information Table 2, this set of hydrogen bonds satisfies

more stringent criteria, including a donor-acceptor distance of 3.1Å and a maximum donor- -acceptor angle of 90°.

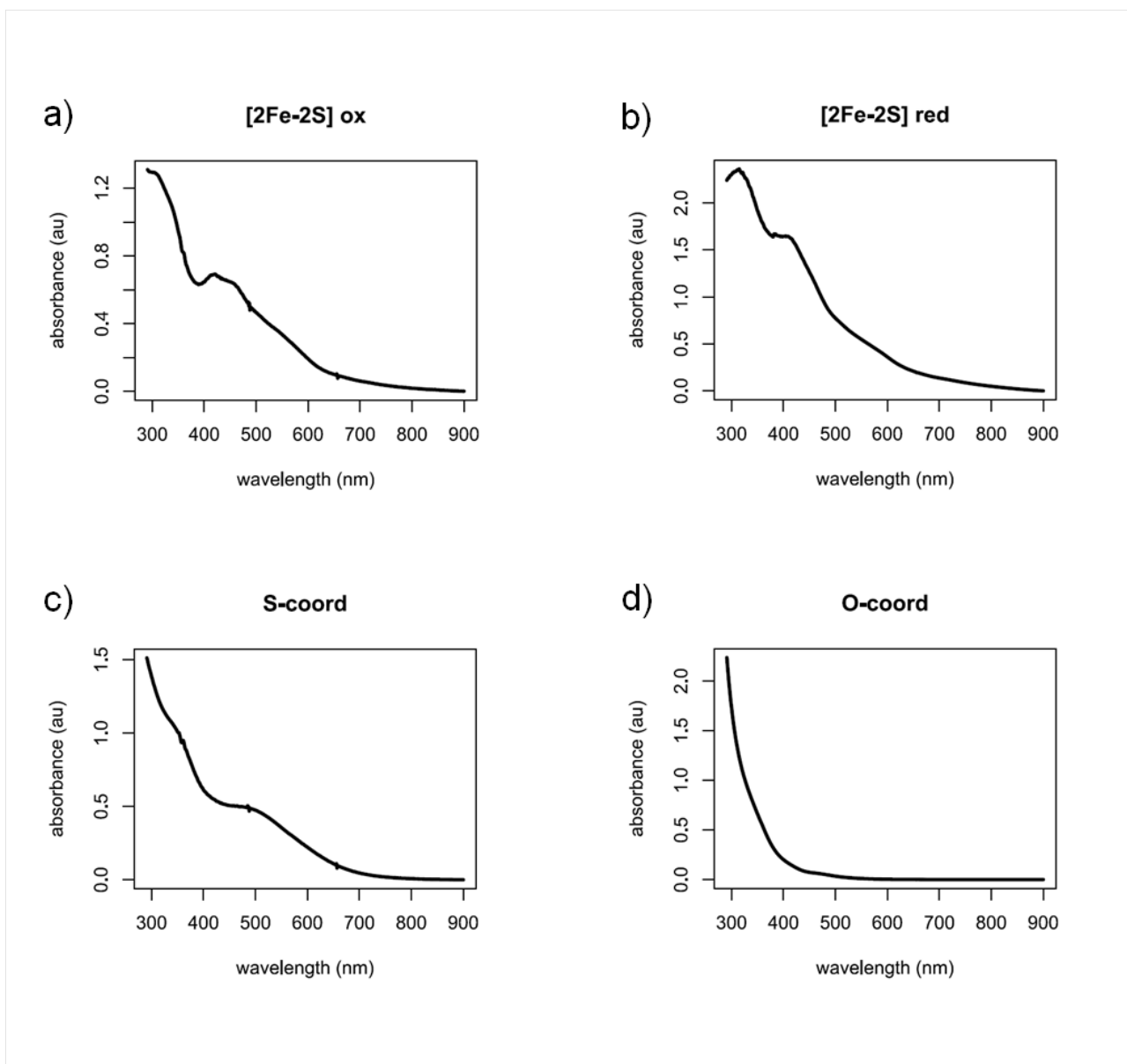
No strong hydrogen bonds were recorded for the entire trajectory, although a strong interaction was recorded between Cysteine and Glutamate.

Residue	Position	H( $\gamma$ -ECG)OH	H( $\gamma$ -ECG) <sub>2</sub> OH	H( $\gamma$ -ECG) <sub>3</sub> OH	H( $\gamma$ -ECG) <sub>4</sub> OH
Glu	$\alpha$	3.59 (1, dd); 53.69 (s)	3.68 (1, b); 53.70(-)  4.13 (1, b); 53.61 (-)	3.59 (1, dd); 54.15 (-)  4.08 (1, b); 54.09 (-)  4.08 (1, b); 54.09 (-)	3.67 (1,- ); 53.82 (-)  4.10 (1, -) 53.88  4.10 (1,-) 53.88  4.10 (1,-); 53.88
	$\beta$	2.02 (2, m); 25.88 (-)	1.83 (2, m); 27.09 (-)  2.04 (2, m); 25.72 (-)	1.85 (2, m); 27.10 (-)  2.01 (2, m); 26.55 (-)  2.06 (2, m); 27.16 (-)	1.85/2.08 (-); 27.42 (-)  1.85 (-); 26.94 (-)  2.06 (-); 25.81 (-)  2.10 (-); 27.28 (-)
	$\gamma$	2.42 (2, m); 31.07 (s)	2.39(2, m); 27.38(-)	2.29 (); 31.54 (-)	2.30 (2, ); 31.46 (-)

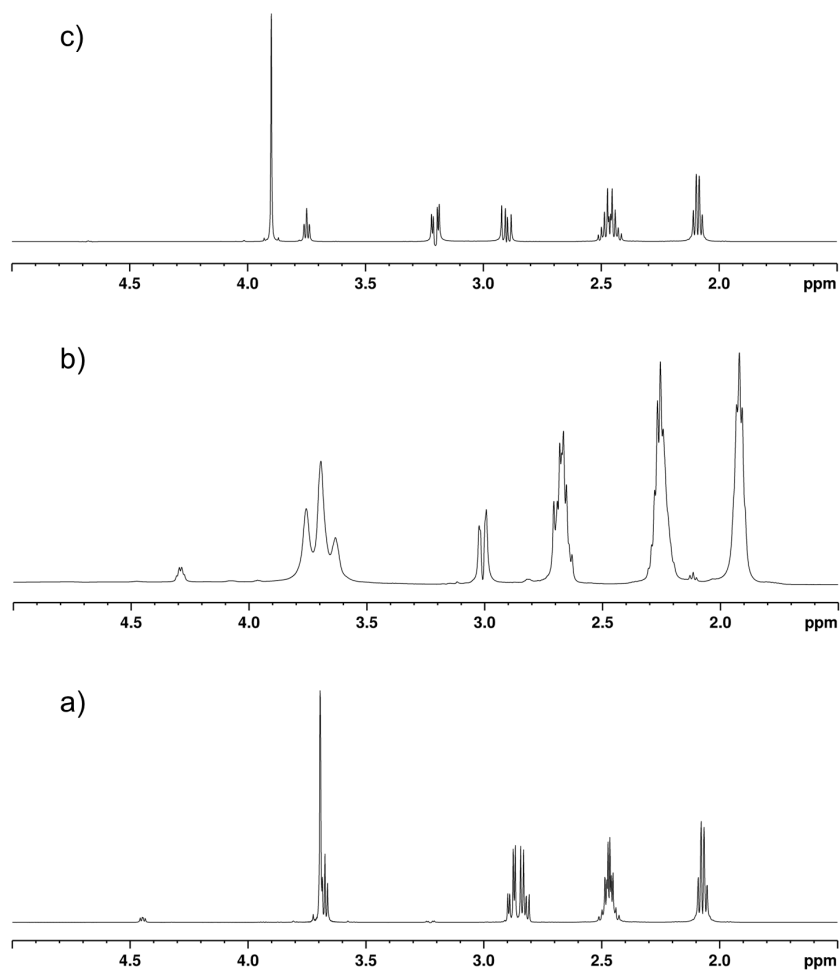
Glu	$\gamma$		2.30(2; m); 31.35(-)	2.29 (); 31.54 (-)  2.42 (); 31.05 (-)	2.30 (2, ); 31.46 (-)  2.30 (2, ); 31.46 (-)  2.47 (2, ); 30.90 (-)
Cys	$\alpha$	4.38 (1,dd); 55.55 (s)	4.46 (1, m); 55.54 (-)  4.48 (1, m); 55.07 (-)	4.35 (1,); 56.42 (-)  4.40 (1,); 56.14 (-)  4.42 (1,-); 55.72 (-)	4.39 (2, m) 55.47 (-)  4.47 (2, m) 55.47 (-)  4.47 (2, m) 55.47 (-)
	$\beta$	2.82 (2,m); 25.26 (-)	2.86 (2, m); 25.20 (-)  2.86 (2; m); 25.20 (-)	2.84 (2, -); 25.58 (-)  2.84 (2, ); 25.58 (-)  2.84 (2, ); 25.58 (-)	2.86 (2, m) 25.12 (-)  2.86 (2, m) 25.12 (-)  2.86 (2, m) 25.12 (-)

Cys	$\beta$				2.86 (2, m) 25.12 (-)
Gly	-	3.67 (2,d); 41.40 (s)	3.88 (1, dd); 42.32 (s)  3.68 (1, m); 42.80 (s)	3.67 (2, s); 42.97 (-)  3.89 (2, m); 42.43 (-)  3.89 (2, m); 42.43 (-)	3.69 (2, ); 42.93 (-)  3.91 (2,); 42.32(-)  3.91 (2,); 42.32(-)  3.91 (2,); 42.32(-)

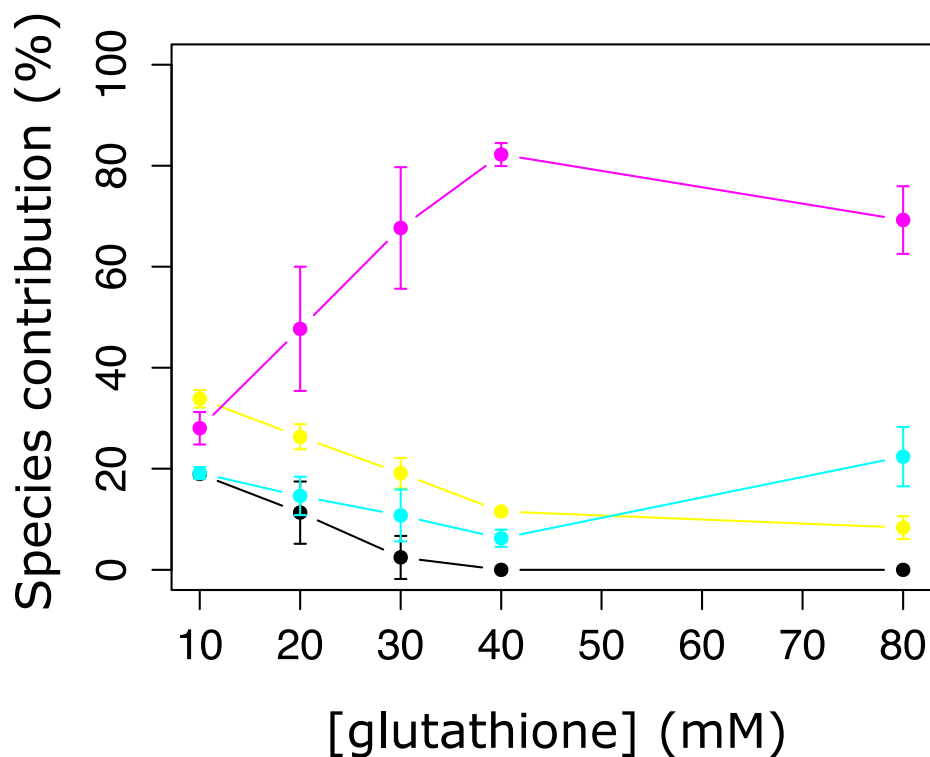
**Supplementary Table 3. NMR spectroscopic data for peptides in D<sub>2</sub>O.** The chemical shift of the N-terminal Glu residue and C-terminal Gly ( $\delta^1\text{H}_{(n, \text{mult})}$ ;  $\delta^{13}\text{C}_{(\text{mult})}$ ) are shown in green and red, respectively. See Supplemental Fig.s S13-S15 for corresponding NMR spectra.



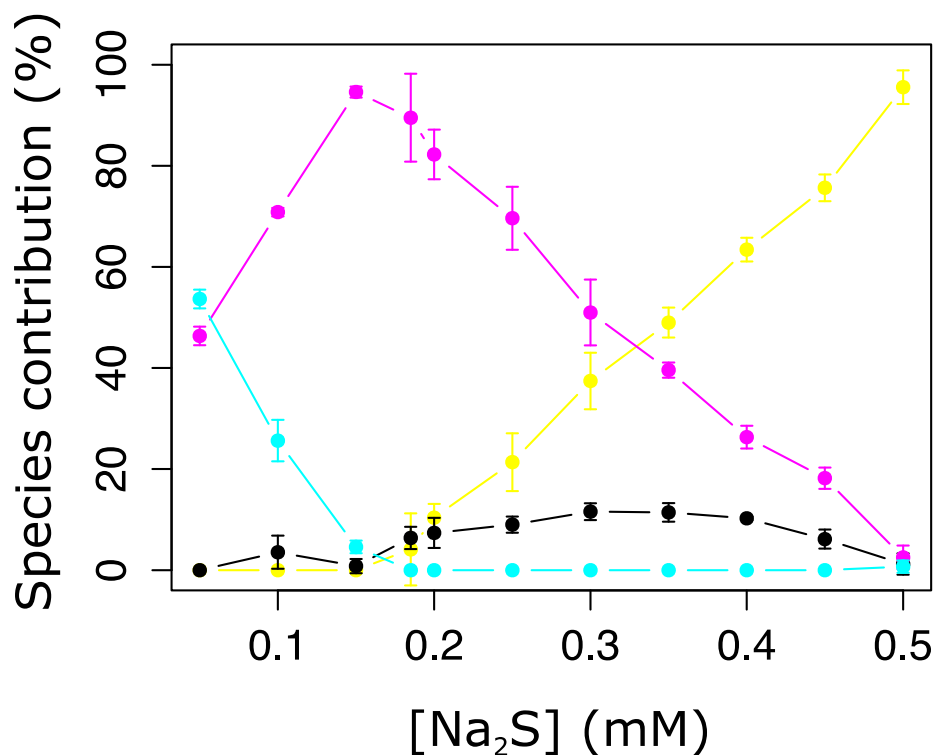
**Supplementary Fig. S1.** UV-Visible absorption spectra of the four reference species used for UV-Visible spectral decomposition. a) oxidized form of [2Fe-2S] glutathione; b) reduced form of [2Fe-2S] glutathione c) rubredoxin-like glutathione/Fe complex (S-coordination to iron); d) oxidized glutathione/Fe complexes (O-coordination to iron).



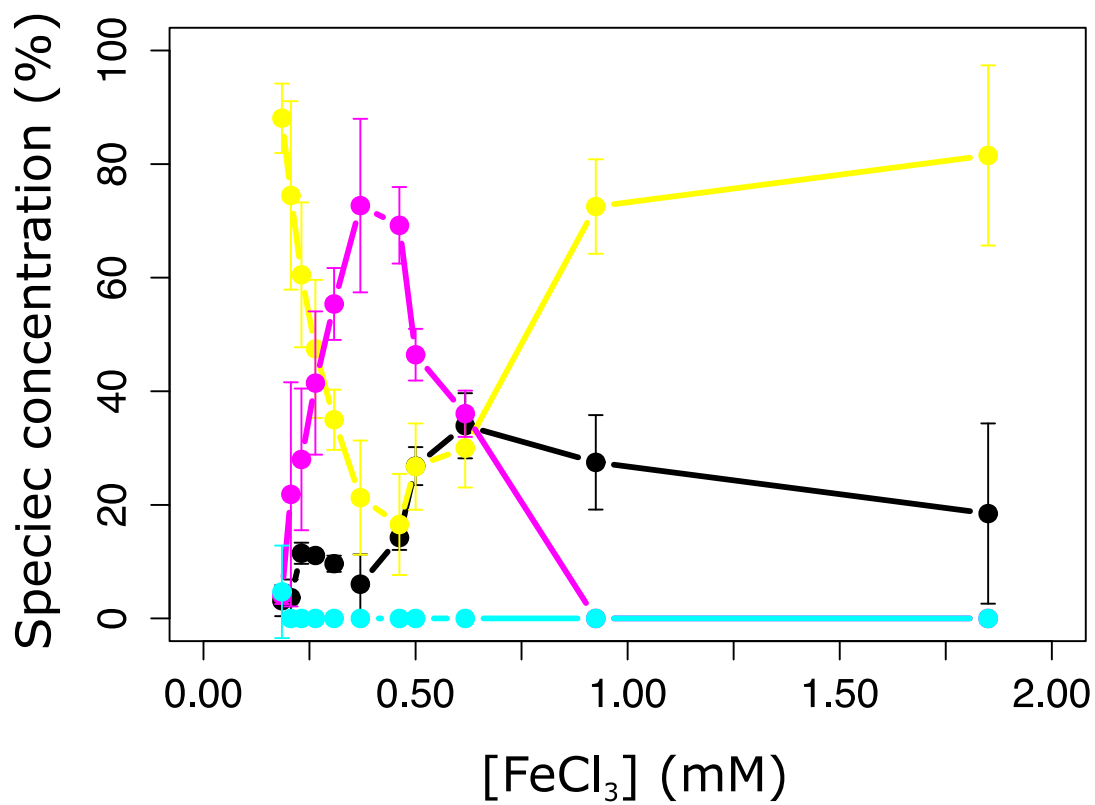
**Supplementary Fig. S2.**  $^1\text{H}$  NMR spectra of **a)** glutathione (40 mM glutathione, pH 8.6), **b)** mixture of glutathione/ $\text{S}^{2-}$ / $\text{Fe}^{3+}$  (40 mM glutathione, ratio 2:1:1, pH 8.6, dil. 100/1) and **c)** oxidized glutathione/ $\text{Fe}^{2+}$  (20 mM oxidized glutathione, ratio 2:1, pH 8.6) in  $\text{D}_2\text{O}$ .



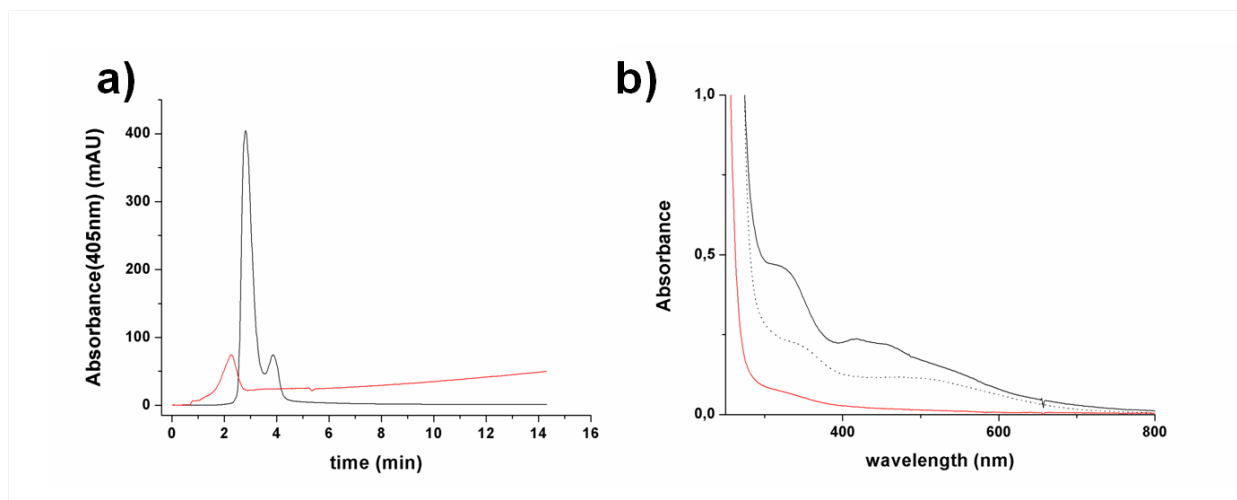
**Supplementary Fig. S3.** Spectral decomposition of the glutathione titration with fixed iron and sulfide concentrations (0.5 mM FeCl<sub>3</sub>, 0.185 mM Na<sub>2</sub>S, pH 8.6). A maximum in oxidized [2Fe-2S] glutathione (magenta) is found at 40 mM. At this concentration, the other three components, oxidized glutathione/Fe complexes (cyan), reduced [2Fe-2S] glutathione (yellow) and mononuclear glutathione/Fe complex (black), exhibit a minimum in composition. Data shown are averages of measurements on three independently run reactions with error bars signifying standard deviation.



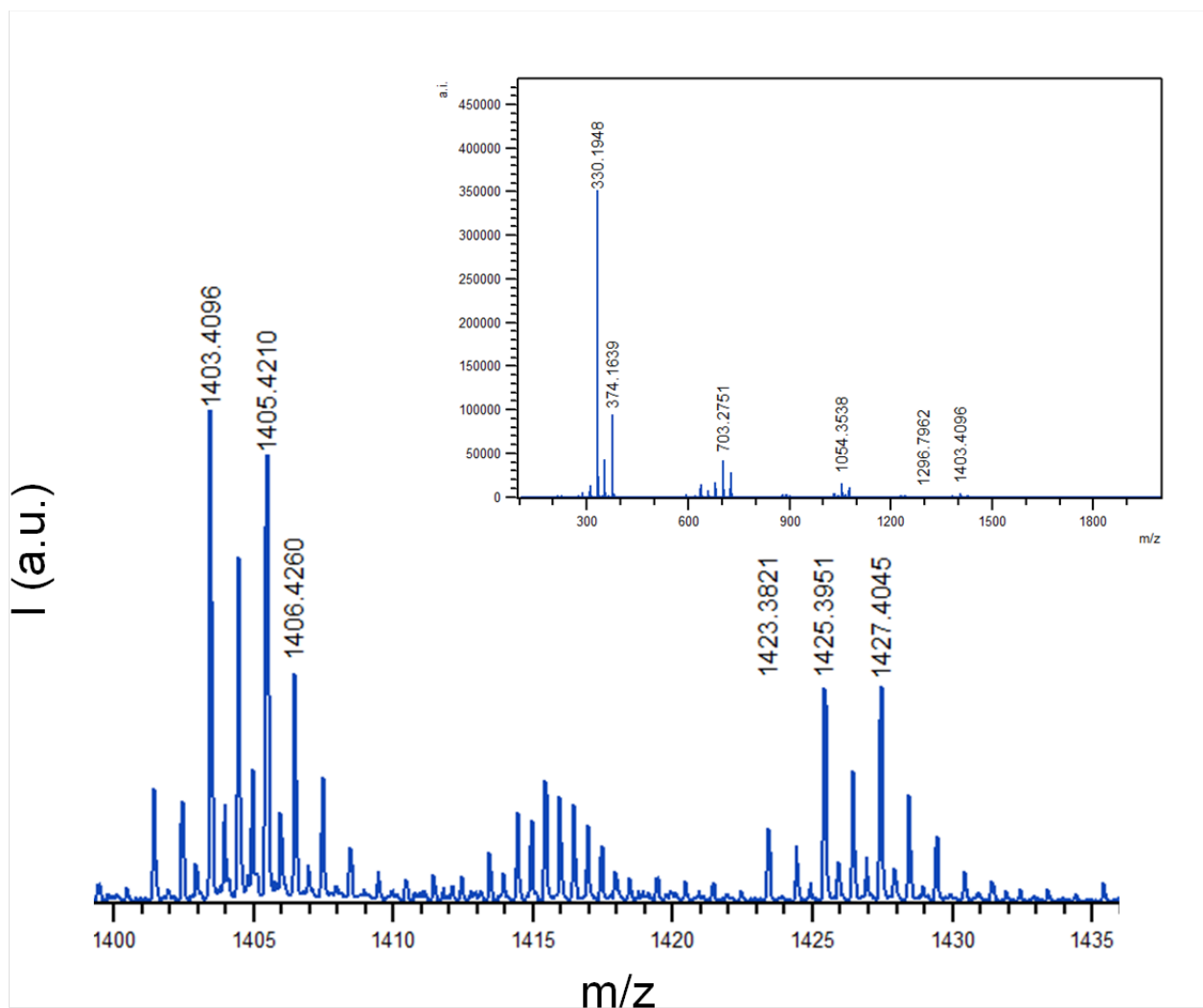
**Supplementary Fig. S4.** Spectral decomposition of the sulfide titration with fixed glutathione and iron concentrations (40 mM glutathione, 0.5 mM FeCl<sub>3</sub>, pH 8.6). A maximum in oxidized [2Fe-2S] glutathione (magenta) is found at about 0.185 mM. At this concentration, the other three components, oxidized glutathione/Fe complexes (cyan), reduced [2Fe-2S] glutathione (yellow) and mononuclear glutathione/Fe complex (black), exhibit a minimum in composition. Data shown are averages of measurements on three independently run reactions with error bars signifying standard deviation.



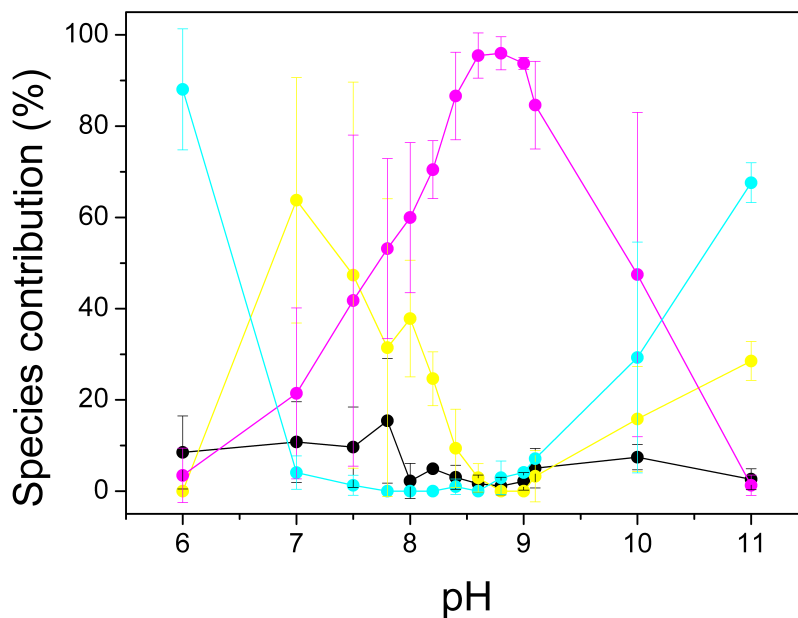
**Supplementary Fig. S5.** Spectral decomposition of the iron titration with fixed glutathione and sulfide concentrations (40 mM glutathione, 0.185 mM Na<sub>2</sub>S, pH 8.6). A maximum in oxidized [2Fe-2S] glutathione (magenta) is found at about 0.5 mM. The other three components are oxidized glutathione/Fe complexes (cyan), reduced [2Fe-2S] glutathione (yellow) and mononuclear glutathione/Fe complex (black). Data shown are averages of measurements on three independently run reactions with error bars signifying standard deviation.



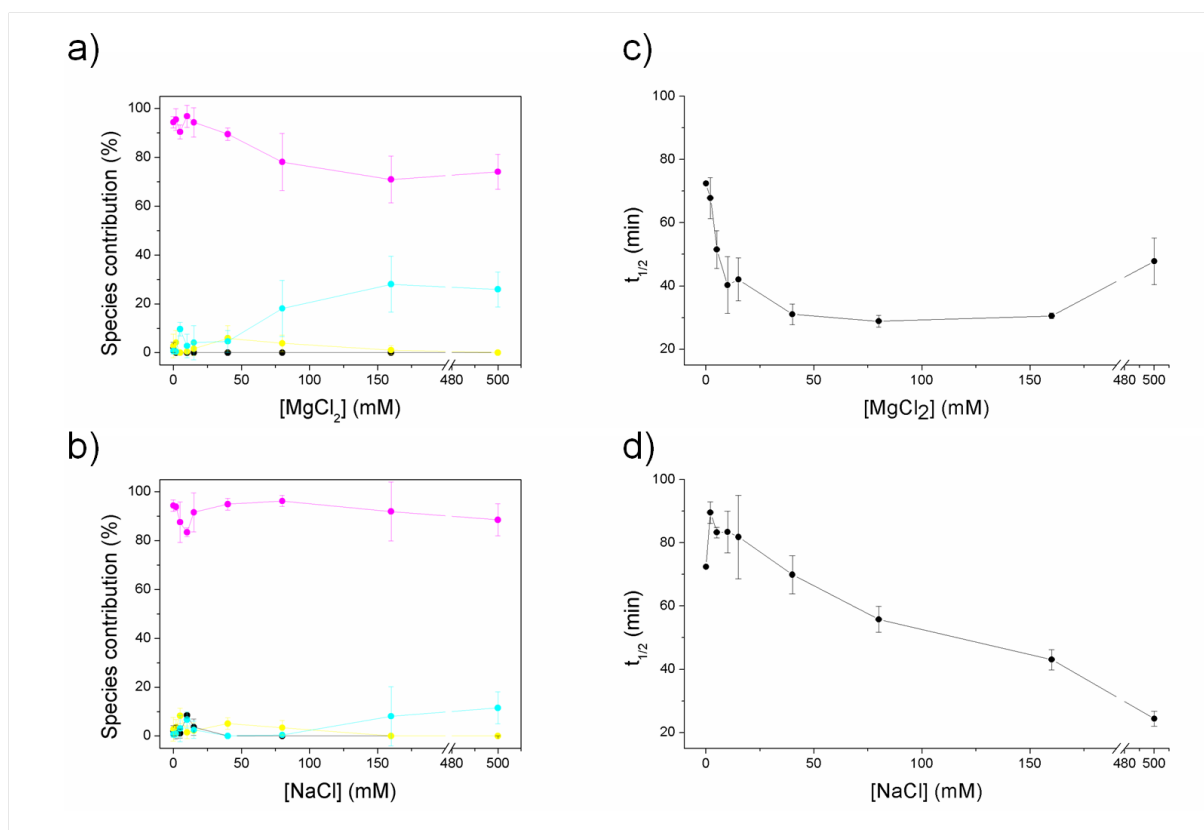
**Supplementary Fig. S6. a)** Comparison of chromatograms of [2Fe-2S] glutathione eluted from a glutathione column (GSTrap) by using 40 mM glutathione, pH 8.6 (black line) and water (red line) as eluent. **b)** UV spectra of the fractions eluted. When the mixture is eluted with 40 mM glutathione pH 8.6 (a, black line), two discrete peaks are detected, corresponding to the elution of [2Fe-2S] glutathione (b, black solid line) and ferric glutathione mononuclear complex (b, black dashed line), respectively. None of the two species is isolated if the running buffer lacks glutathione (b, red line).



**Supplementary Fig. S7.** Mass spectra of the reaction mixture containing glutathione, sodium sulfide and ferric chloride. A family of peaks corresponding to oxidized [2Fe-2S] glutathione (1425  $m/z$  and 1403.4, that is  $[M+Na^+]$  and  $[M+2H^+]$  cluster, respectively) are overlapped with signals attributable to mixed valence cluster (1426.4  $m/z$  and 1404.4  $m/z$ , that is, iron sulfur-clusters with  $Na^+$  and  $3H^+$ , respectively) and with signals of glutathione tetramer (1427.4  $m/z$  and 1405.4  $m/z$ ,  $[M+9Na]^+$  and  $[M+8Na+H]^+$ , respectively). The full spectrum is shown in the inset.

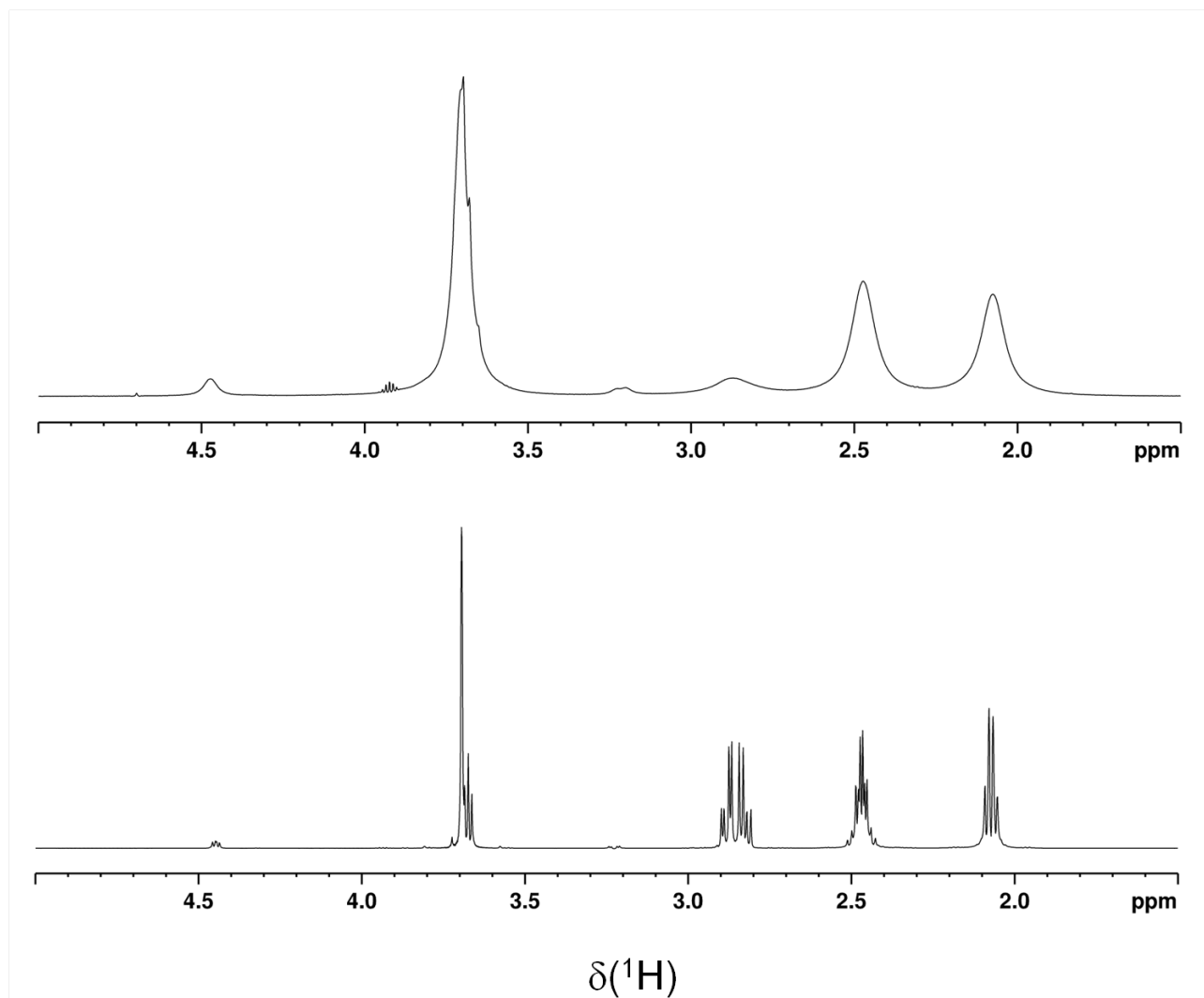


**Supplementary Fig. S8.** The influence of pH on the formation of [2Fe-2S] glutathione (40 mM glutathione, 0.185 mM Na<sub>2</sub>S, 0.5 mM FeCl<sub>3</sub>, variable pH range 7-11) obtained by spectral decomposition. A maximum in oxidized [2Fe-2S] glutathione (magenta) is found at pH 8.6. At this value, the other three components, oxidized glutathione/Fe complexes (cyan), reduced [2Fe-2S] glutathione (yellow) and mononuclear glutathione/Fe complex (black), exhibit a minimum in composition. Data shown are averages of measurements on three independently run reactions with error bars signifying standard deviation.

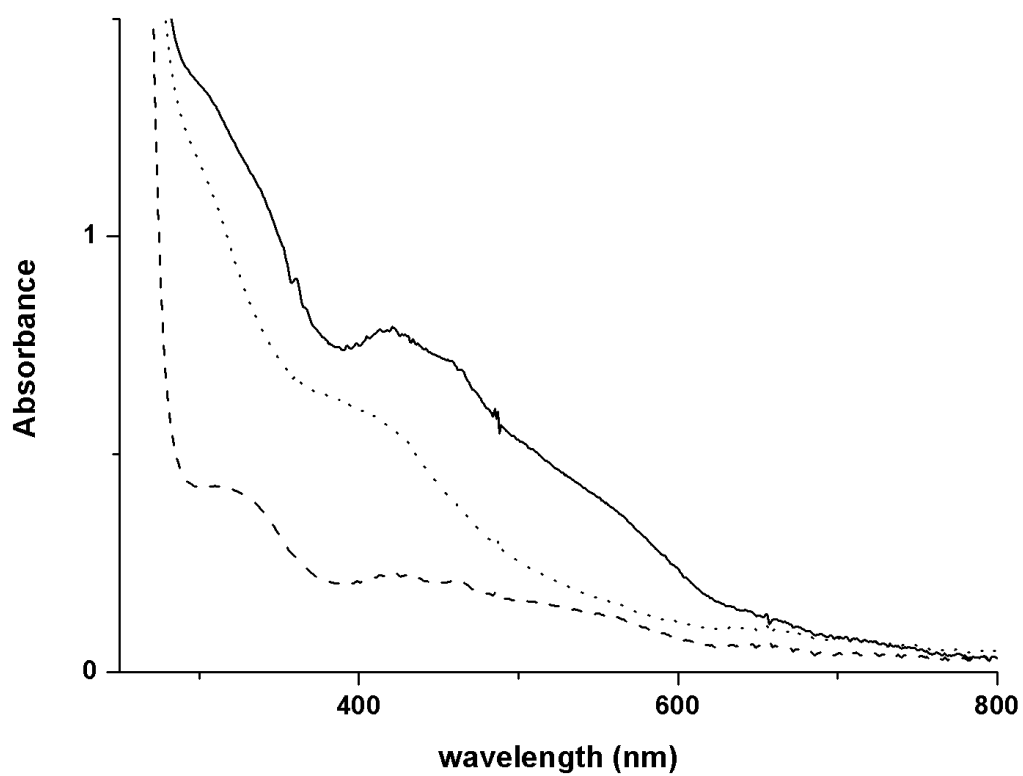


**Supplementary Fig. S9.** Influence of MgCl<sub>2</sub> and NaCl on formation and stability of [2Fe-2S] glutathione.

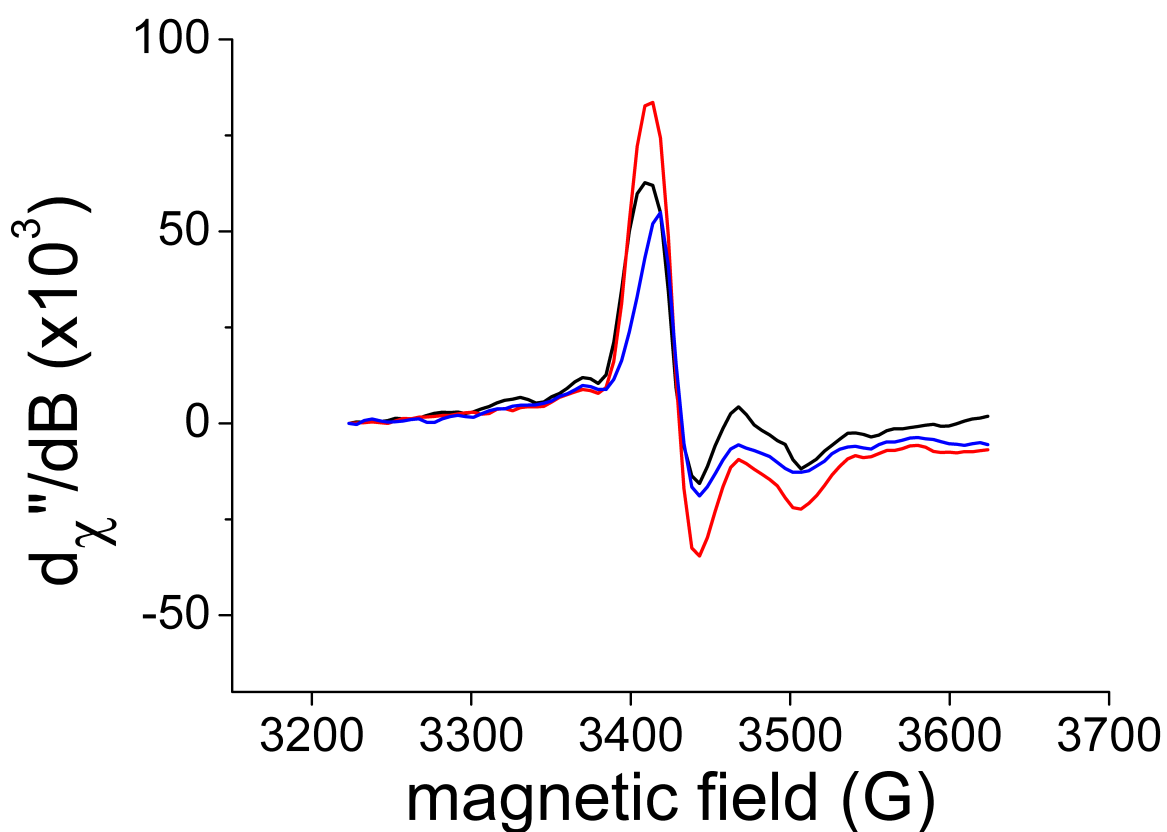
Spectral decomposition of [2Fe-2S] glutathione in the presence of 0-500 mM MgCl<sub>2</sub> (a) and NaCl (b) with glutathione, sulfide, and iron concentrations fixed at the optimal values (40 mM glutathione, 0.185 mM Na<sub>2</sub>S, and 0.5 mM FeCl<sub>3</sub>, pH 8.6). In the figure are shown contribution parameters of oxidized [2Fe-2S] glutathione (magenta), oxidized glutathione/Fe complex (cyan), reduced [2Fe-2S] glutathione (yellow) and mononuclear glutathione/Fe complex (black) to spectra collected one minute after the mixing of the reagents. Half life ( $t_{1/2}$ ) of [2Fe-2S] cluster in presence of 0-500 mM MgCl<sub>2</sub> (c) and NaCl (d). A minimum value of  $t_{1/2}$  is found at 80 mM MgCl<sub>2</sub>, whereas a maximum  $t_{1/2}$  is found in presence of 2 mM NaCl. Data shown are averages of measurements on three independently run reactions with error bars signifying standard deviation.



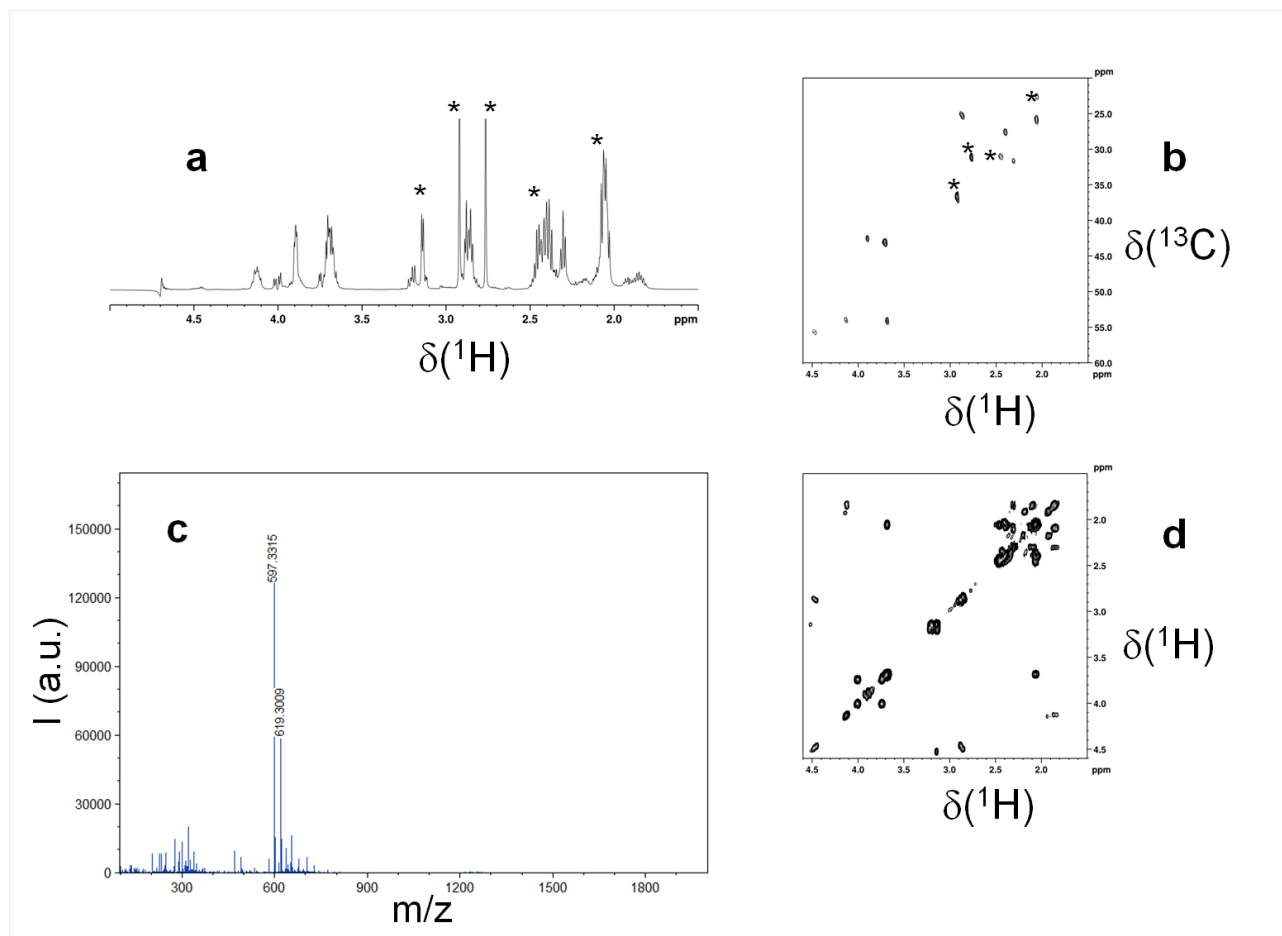
**Supplementary Fig. S10.**  $^1\text{H}$ -NMR diamagnetic spectrum of [2Fe-2S] glutathione (top) and free glutathione (bottom) at pH 8.6. The presence of paramagnetic ions results in a general broadening of the signal. Evidence of the oxidation of glutathione is given by the presence of the signal at 3.2 ppm.



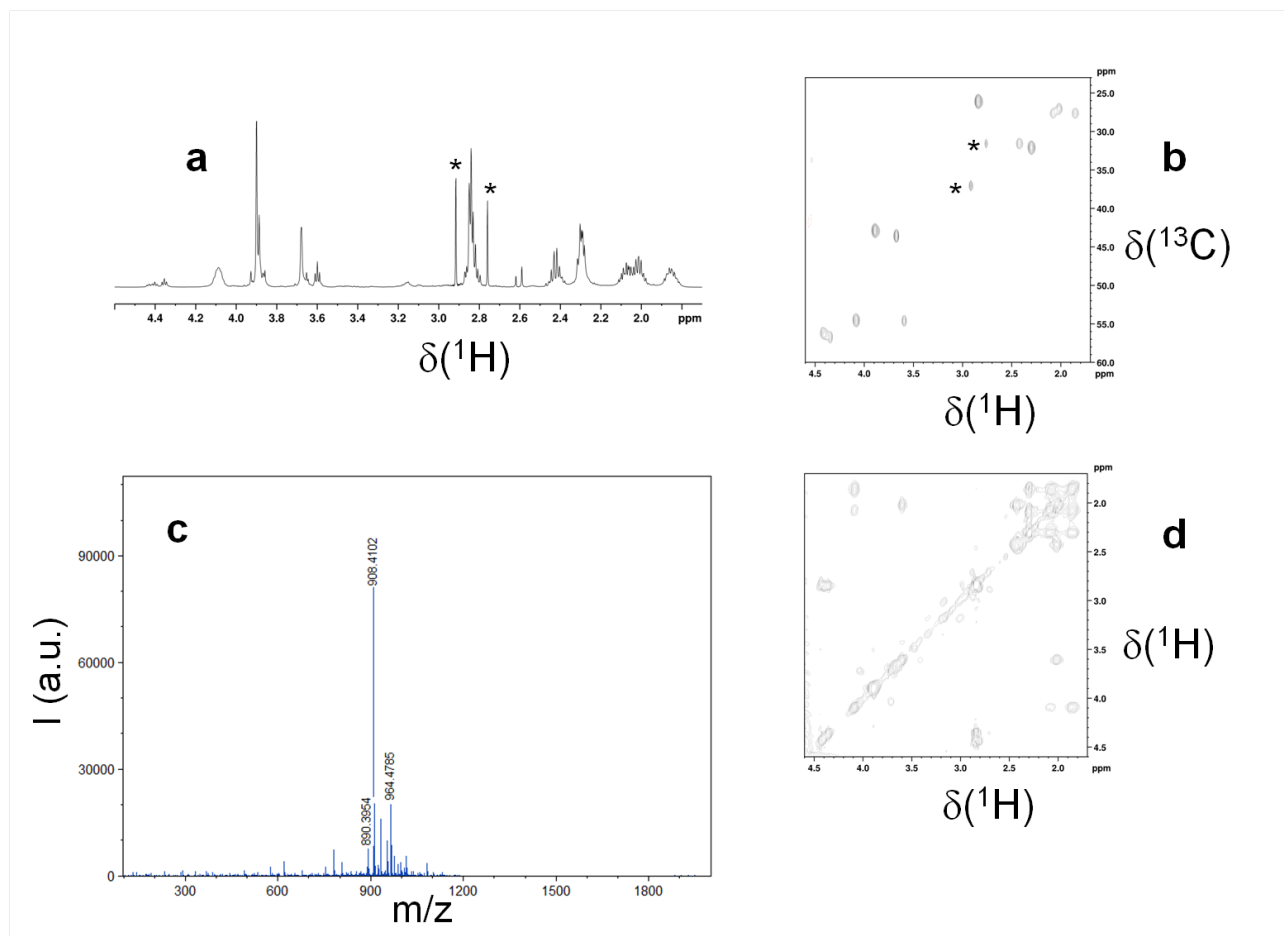
**Supplementary Fig. S11.** UV-Visible absorption spectra of [2Fe-2S] glutathione before (full line) and after the reduction with sodium dithionite (dotted line). After the reduction, the mixture containing [2Fe-2S] glutathione is purified on Sepharose G-10 resin. Upon the addition of hydrogen peroxide to the eluate, it is possible to observe again the bands at 420 and 450 nm distinctive of oxidized [2Fe-2S] cluster (dashed line).



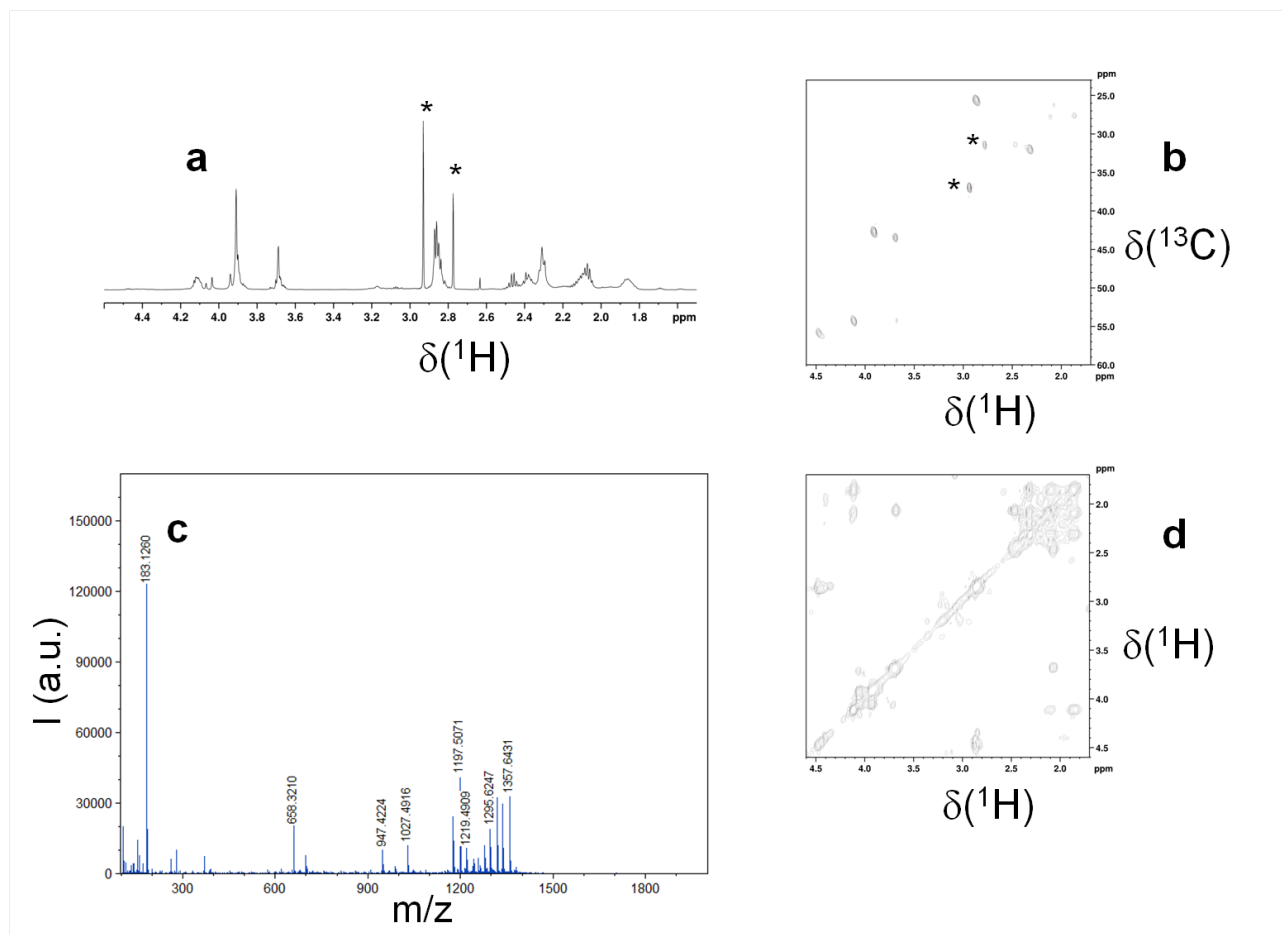
**Supplementary Fig. S12.** EPR spectra of  $[2\text{Fe-2S}]^{1+}$  at variable temperature. The cluster type was confirmed by the relaxation behavior of the signal.  $[2\text{Fe-2S}]^{1+}$  clusters typically exhibit slow relaxation resulting in insignificant broadening at 70 K, whereas  $[4\text{Fe-4S}]^{1+}$  clusters, which show faster relaxation, are only generally observable below 30K.<sup>30</sup> Here, EPR spectra were recorded at 20 K (black), 40 K (red), and 80 K (blue). The signal, still detectable at temperatures higher than 30 K, and the negligible differences in broadening are consistent with the presence of a  $[2\text{Fe-2S}]^{1+}$  cluster.



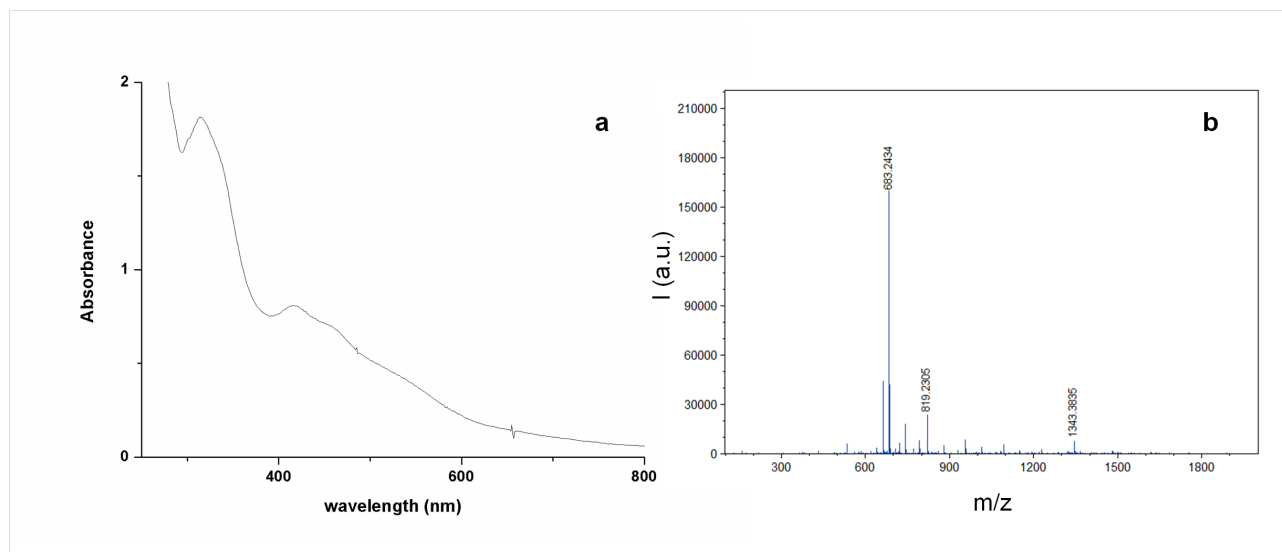
**Supplementary Fig. S13.** Characterization of  $\text{H}_2\text{N}(\gamma\text{-ECG})_2\text{OH}$  (the hexapeptide).  $^1\text{H}$  NMR (a),  $^1\text{H}$ ,  $^{13}\text{C}$  HSQC (b),  $^1\text{H}$ ,  $^1\text{H}$  COSY (d) spectra are shown. The asterisks indicate resonances from TCEP (2.05, 2.39 ppm), DMF (2.76, 2.92 ppm), and EDT (3.17 ppm). High resolution mass spectrum (c) for the  $\text{H}_2\text{N}(\gamma\text{-ECG})_2\text{OH}$  aqueous solution. The peak found at 597.3315 m/z is consistent with the value of the isotopic mass calculated for protonated hexapeptide ( $[\text{M}+1]$ , formula  $\text{C}_{20}\text{H}_{33}\text{N}_6\text{O}_{11}\text{S}_2$ , 597.1649 Da).



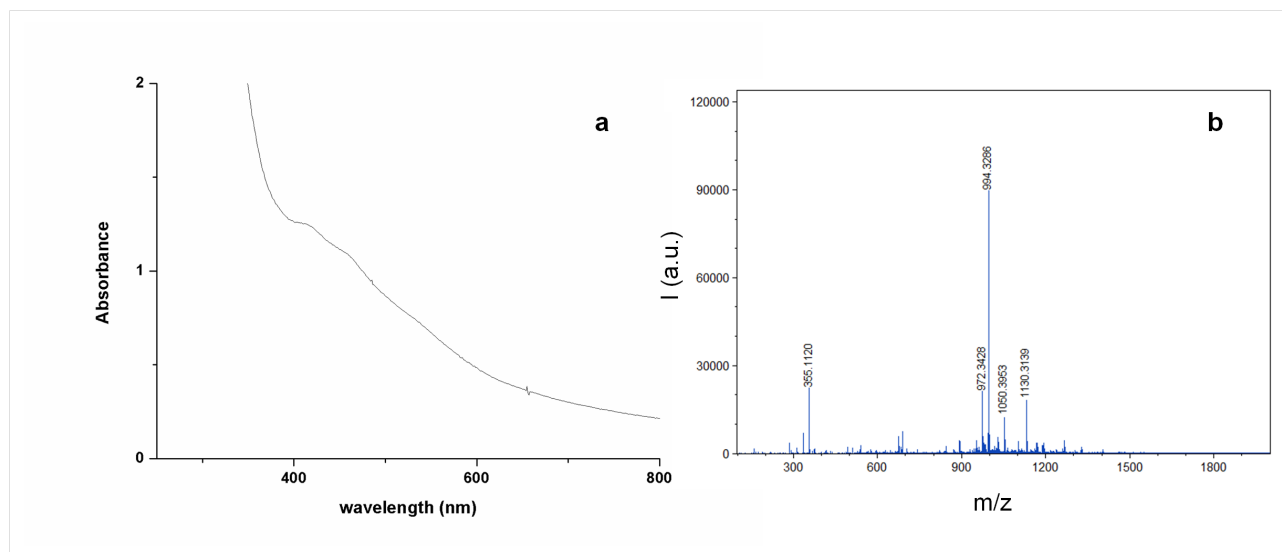
**Supplementary Fig. S14.** Characterization of  $\text{H}_2\text{N}(\gamma\text{-ECG})_3\text{OH}$  (the nonapeptide).  $^1\text{H}$  NMR (a),  $^1\text{H}$ ,  $^{13}\text{C}$  HSQC (b),  $^1\text{H}$ ,  $^1\text{H}$  COSY (d) spectra are shown. The asterisks indicate resonances from DMF (2.76, 2.92 ppm). High resolution mass spectrum (c) for the  $\text{H}_2\text{N}(\gamma\text{-ECG})_3\text{OH}$  aqueous solution. The peak found at 908.4102 m/z is consistent with the value of the isotopic mass calculated for sodium-nonapeptide adduct ( $[\text{M}+\text{Na}]$ , formula  $\text{C}_{30}\text{H}_{47}\text{N}_9\text{O}_{16}\text{S}_3\text{Na}$ , 908.2200 Da).



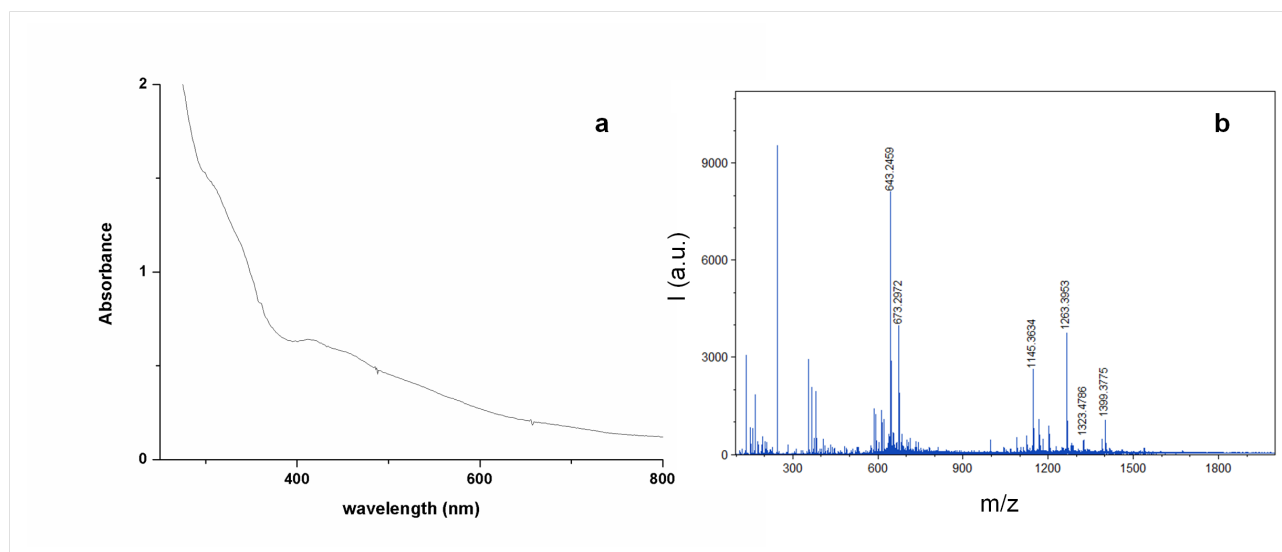
**Supplementary Fig. S15.** Characterization of  $\text{H}_2\text{N}(\gamma\text{-ECG})_4\text{OH}$  (the dodecapeptide).  $^1\text{H}$  NMR (a),  $^1\text{H}$ ,  $^{13}\text{C}$  HSQC (b),  $^1\text{H}$ ,  $^1\text{H}$  COSY (d) spectra are shown. Asterisks indicate resonances from DMF (2.76, 2.92 ppm). High resolution mass spectrum (c) for the  $\text{H}_2\text{N}(\gamma\text{-ECG})_4\text{OH}$  aqueous solution. The peak found at 1197.5071 m/z is consistent with the value of isotopic mass calculated for sodium-dodecapeptide adduct ( $[\text{M}+\text{Na}]$ , formula  $\text{C}_{40}\text{H}_{62}\text{N}_{12}\text{O}_{21}\text{S}_4\text{Na}$ , 1197.2933 Da).



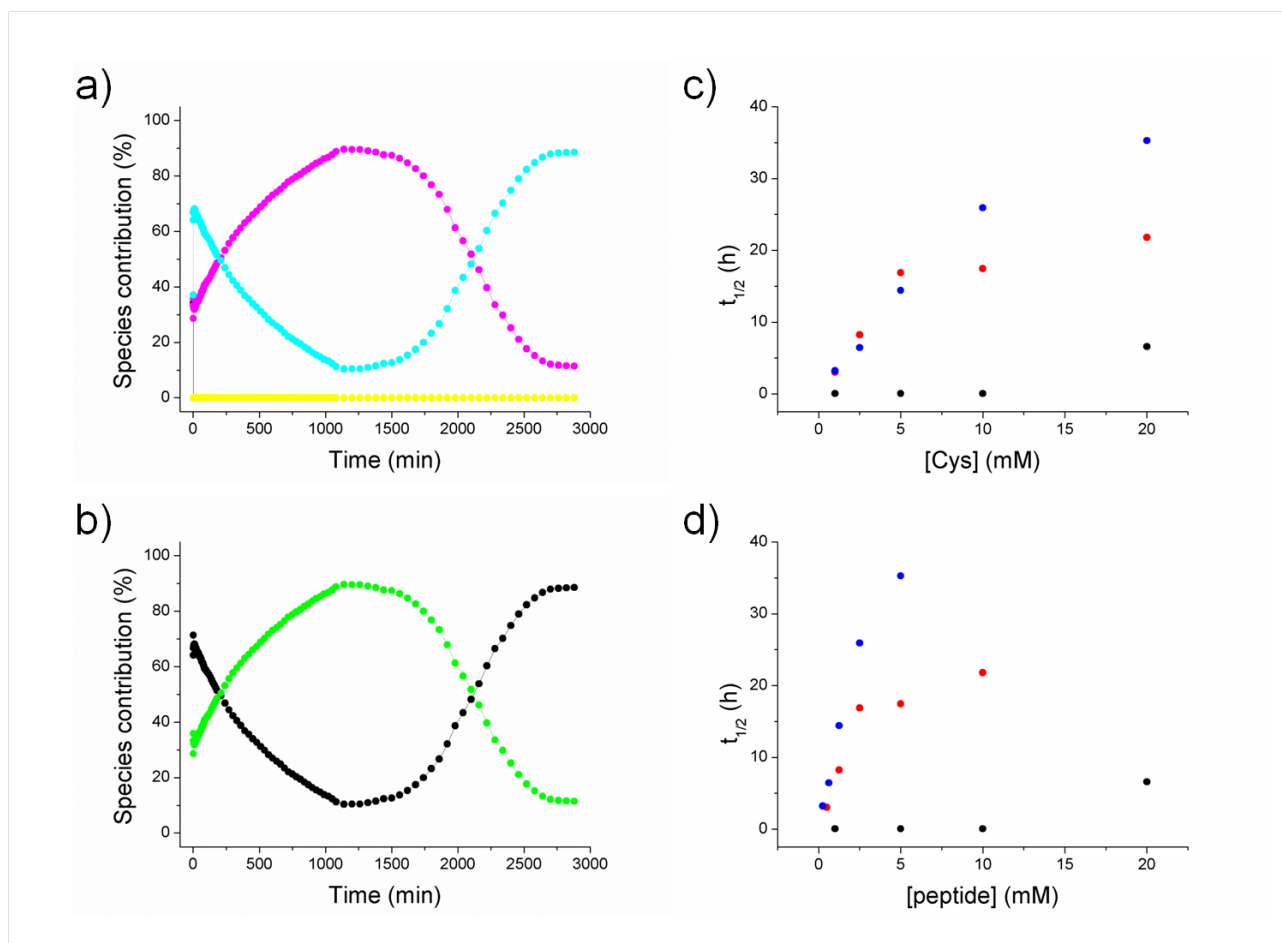
**Supplementary Fig. S16.** Characterization of [2Fe-2S] hexapeptide,  $\text{H}_2\text{N}(\gamma\text{-ECG})_2\text{OH}$ . UV-Visible absorption spectrum for the complex (a) shows the characteristic bands at 420 and 450 nm. (b) High resolution mass spectrum for the  $\text{H}_2\text{N}(\gamma\text{-ECG})_2\text{OH}$  [2Fe-2S] cluster solution. The peak found at 683.2434 m/z is consistent with the value of isotopic mass calculated for a double charged adduct ( $[\text{2M-2+2Fe+2S}]^{2+}$ , M = hexapeptide; formula  $\text{C}_{40}\text{H}_{63}\text{N}_{12}\text{O}_{22}\text{S}_6\text{Fe}_2$ , 683.5601 Da).



**Supplementary Fig. S17.** Characterization of [2Fe-2S] nonapeptide,  $\text{H}_2\text{N}(\gamma\text{-ECG})_3\text{OH}$ . UV-Visible spectrum for the mixture (a) shows the characteristic bands at 420 and 450 nm. (b) High resolution mass spectrum for the  $\text{H}_2\text{N}(\gamma\text{-ECG})_3\text{OH}$  [2Fe-2S] cluster solution. The peaks found at 972.3428 and 994.3286 m/z are consistent with the value of isotopic mass calculated for a monpositive adduct nonapeptide-Fe-S ( $[\text{M}-1+\text{Fe}+\text{S}]^+$ , formula  $\text{C}_{30}\text{H}_{46}\text{N}_9\text{O}_{16}\text{S}_4\text{Fe}$ , 972.1295 Da) and its adduct with the a sodium ion ( $[\text{M}-2+\text{Fe}+\text{S}+\text{Na}]^+$ , M = nonapeptide; formula.  $\text{C}_{30}\text{H}_{45}\text{N}_9\text{O}_{16}\text{S}_4\text{FeNa}$ , 994.1114 Da). These adducts could be considered as a product of the degradation of a [2Fe-2S] cluster stabilized by the nonapeptide.



**Supplementary Fig. S18.** Characterization of [2Fe-2S] dodecapeptide,  $\text{H}_2\text{N}(\gamma\text{-ECG})_4\text{OH}$ . UV-Visible spectrum of the mixture (a) shows the characteristic bands at 420 and 450 nm. (b) High resolution mass spectrum for the  $\text{H}_2\text{N}(\gamma\text{-ECG})_4\text{OH}$  [2Fe-2S] cluster solution. The peak found at 673.2974 m/z is consistent with the value of isotopic mass calculated for a double charged [2Fe-2S] cluster stabilized by the dodecapeptide ( $[\text{M}-4+2\text{Fe}+2\text{S}]^{2+}$ , M = dodecapeptide; formula  $\text{C}_{40}\text{H}_{58}\text{N}_{12}\text{O}_{21}\text{S}_6\text{Fe}_2$ , 673.0478 Da).



**Supplementary Fig. S19.** Determination of  $t_{1/2}$  for [2Fe-2S] stabilized by peptides at different concentrations of cysteinyl ligand. As an example, the decomposition of UV-Visible absorption spectra acquired in the course of time is reported (a) for a solution of [2Fe-2S] hexapeptide (10 mM hexapeptide, 0.1 mM sodium sulfide, 0.25 mM ferric chloride, pH 8.6). The contribution parameters of oxidized [2Fe-2S] (magenta), reduced [2Fe-2S] (yellow), S-coordinated glutathione/Fe complex (black), O-coordinated oxidized glutathione/Fe complex (cyan) were used to calculate the overall contribution of both cluster and non-cluster species (b, green and black, respectively). The set of  $t_{1/2}$  calculated with the fitting for each peptide at different concentrations of cysteinyl ligand was plotted in a graph time vs [cys] and time vs [peptide] (c and d, respectively; black, glutathione; red, hexapeptide and blue, dodecapeptide clusters).

## Supplementary References

- 1 R Development Core Team, *R: a language and environment for statistical computing*, R Foundation for Statistical Computing, Wienn, Austria, 2011.
- 2 A. Isidro-Llobet, M. Álvarez and F. Albericio, *Chem. Rev.*, 2009, **109**, 2455–2504.
- 3 K. J. Jensen, P. T. Shelton and S. L. Pedersen, *Peptide synthesis and applications*, Humana press, New York, Second edition., 2013, vol. 1047.
- 4 C. Kaszuba, P. A. Postila, O. Cramariuc, M. Sarewicz, A. Osyczka, I. Vattulainen and T. Róg, *Theor. Chem. Acc.*, 2013, **132**, 1370.
- 5 M. S. Gordon and M. W. Schmidt, in *Theory and Applications of Computational Chemistry: The First Forty Years*, (Dykstra C.E., Frenking G., Scuseria G.E.), Elsevier B.V., Amsterdam, 2005, pp. 1167–1189.
- 6 B. M. Bode and M. S. Gordon, *J. Mol. Graph. Model.*, 1998, **16**, 133–138.
- 7 M. D. Hanwell, D. E. Curtis, D. C. Lonie, T. Vandermeersch, E. Zureck and G. R. Hutchison, *J. Cheminformatics*, 2012, **4**.
- 8 A. A. Granovsky, Firefly version 8, [www http://classic.chem.msu.su/gran/firefly/index.html](http://classic.chem.msu.su/gran/firefly/index.html).
- 9 P. E. M. Siegbahn and M. R. A. Blomberg, *Chem. Rev.*, 2000, **100**, 421–437.
- 10 U. Ryde, M. H. M. Olsson and K. Pierloot, *Theor. Comput. Chem.*, 2001, **9**, 1–56.
- 11 A. Schäfer, H. Horn and R. Ahlrichs, *J. Chem. Phys.*, 1992, **97**, 2571–2577.
- 12 D. Feller, *J. Comput. Chem.*, 1996, **17**, 1571–1586.
- 13 K. L. Schuchardt, B. T. Didier, T. Elsethagen, L. Sun, V. Gurumoorthi, J. Chase, J. Li and T. L. Windus, *J. Chem. Inf. Model.*, 2007, **47**, 1045–1052.
- 14 B. Mennucci, *Wiley Interdiscip. Rev. Comput. Mol. Sci.*, 2012, **2**, 386–404.
- 15 R. D. Shannon, *Acta Crystallogr. A*, 1976, **32**, 751–767.
- 16 L. Noodleman, D. A. Case and A. Aizman, *J. Am. Chem. Soc.*, 1988, **110**, 1001–1005.
- 17 J. A. Boatz and M. S. Gordon, *J. Phys. Chem.*, 1989, **93**, 1819–1826.
- 18 K. H. Merz, *J. Comput. Chem.*, 1992, **13**, 749–767.
- 19 U. Chandra Singh and P. A. Kollman, *J. Comput. Chem.*, 1984, **5**, 129–145.
- 20 B. R. Brooks, R. E. Brucolieri, B. D. Olafson, D. J. States, S. Swaminathan and M. Karplus, *J. Comput. Chem.*, 1983, **4**, 187–217.
- 21 B. R. Brooks, C. L. Brooks, III, A. D. Mackerell, Jr., L. Nilsson, R. J. Petrella, B. Roux, Y. Won, G. Archontis, C. Bartels, S. Boresch, A. Cafflich, L. Caves, Q. Cui, A. R. Dinner, M. Feig, S. Fischer, J. Gao, M. Hodoscek, W. Im, K. Kuczera, T. Lazaridis, J. Ma, V. Ovchinnikov, E. Paci, R. W. Pastor, C. B. Post, J. Z. Pu, M. Schaefer, B. Tidor, R. M. Venable, H. L. Woodcock, X. Wu, W. Yang, D. M. York and M. Karplus, *J. Comput. Chem.*, 2009, **30**, 1545–1614.
- 22 A. D. MacKerell Jr., C. L. Brooks, III, L. Nilsson, B. Roux, Y. Won and M. Karplus, in *The Encyclopedia of Computational Chemistry*, John Wiley & Sons, Chichester, 1998, vol. 1, pp. 271–277.
- 23 J. C. Phillips, R. Braun, W. Wang, J. Gumbart, E. Tajkhorshid, E. Villa, C. Chipot, R. D. Skeel, L. Kalé and K. Schulten, *J. Comput. Chem.*, 2005, **26**, 1781–1802.
- 24 E. F. Pettersen, T. D. Goddard, C. C. Huang, G. S. Couch, D. M. Greenblatt, E. C. Meng and T. E. Ferrin, *J. Comput. Chem.*, 2004, **25**, 1605–1612.
- 25 J.-P. Ryckaert, A. Bellemans, G. Ciccotti and G. V. Paolini, *Phys. Rev. Lett.*, 1988, **60**, 128–131.
- 26 U. Essmann, L. Perera, M. L. Berkowitz, T. Darden, H. Lee and L. G. Pedersen, *J. Chem. Phys.*, 1995, **103**, 8577–8593.
- 27 W. Humphrey, A. Dalke and K. Schulten, *J. Mol. Graph.*, 1996, **14**, 33–38.
- 28 V. A. Voelz, G. R. Bowman, K. Beauchamp and V. S. Pande, *J. Am. Chem. Soc.*, 2010, **132**, 1526–1528.
- 29 I. K. McDonald and J. M. Thornton, *J. Mol. Biol.*, 1994, **238**, 777–793.
- 30 M. K. Johnson, in *Encyclopedia of Inorganic Chemistry*, (King R. B.), John Wiley & Sons, Chichester, UK, 1994, pp. 1896–1915.